Phenotypic Differences in Adult and Fetal Dermal Fibroblast Responses to Mechanical Tension

Umang M. Parikh[1,*], Walker D. Short[1,*], Natalie Templeman[1], Alexander Blum[1], Daniel Colchado[1], Harrison Strang[1], Aditya Kaul[1], Hui Li[1], Xinyi Wang[1], Monica M. Fahrenholtz[1], Swathi Balaji[1]

[1] Laboratory for Regenerative Tissue Repair, Division of Pediatric Surgery, Department of Surgery, Texas Children's Hospital and Baylor College of Medicine, Houston, TX, 77030, USA

*Equally Contributing Authors

Corresponding author:

Swathi Balaji

Feigin Center, C.450.05

1102 Bates Avenue

Texas Children's Hospital and Baylor College of Medicine

Phone: (832) 824-0461

Fax: (832) 825-3141

Email: balaji@bcm.edu

The authors declare no competing financial interests.

Short Title: Fibroblast Responses to Mechanical Tension

Keywords: fetal, regenerative wound healing, mechanical tension, stretch, scarring, fibrosis, fibroblasts, hyaluronan, ECM, wound tension

ABSTRACT

The regenerative wound healing phenotype observed in the fetal wounds is characterized by a unique hyaluronan rich wound microenvironment. Fetal fibroblasts produce a pericellular matrix which is abundant in high molecular weight HA. In vivo, fetal skin has negligible resting tension and heals regeneratively when small wounds are made. However, critically large fetal wounds heal with increased scar. We hypothesize that higher mechanical tension will differentially alter fibroblast-mediated HA metabolism in adult and fetal fibroblasts, leading to a profibrotic fetal fibroblast phenotype. C57BL/6J fetal (FFB, E14.5) and adult (AFB, 8 wk) dermal fibroblasts were cultured on silicone membranes +/-10% static strain (1, 3, 6, and 12h). Monolayers were analyzed via PCR for HA-synthesis (HAS1-3), HA-remodeling (HYAL1-2, KIAA1199), and HA-receptor (CD44) genes, normalized to static FFB. Total HA was analyzed by gel electrophoresis at 12h. Data is reported as mean+/-SD (n=3), with p-values calculated by two-way ANOVA (post-hoc Tukey's test). FFB pericellular matrix was reduced after tension conditions, and HA profile shifted from HMW-HA to LMW-HA. Under static conditions, AFB had increased expression of HAS 1 and 2, as well as increased expression of KIA1199, HYAL1 and 2 when compared to FFB. Overall, tension resulted in an increase in HAS1, HAS3, and HYAL1 expression in FFB, and decreased HAS2 but increased HYAL1 for AFB under tension. Staining for cytoskeletal components demonstrates that tension results in organization of F-actin and aSMA in FFB to resemble AFB. Expression of aSMA is increased in AFB with tension, while CD26 expression is increased in FFB with tension. These insights into the intrinsic differences between regenerative FFB and fibrotic AFB may yield targets to attenuate fibrosis.

Introduction

Cutaneous wounds in the mid-gestation mammalian fetus heal regeneratively, with wound repair indistinguishable from the surrounding uninjured skin. Significant work has been done to identify the key contributors to the regenerative wound healing responses in the fetus. Among these critical factors are abundant and sustained levels of hyaluronan (HA) content and low expression of fibrogenic and inflammatory cell and cytokine responses in the wound microenvironment in the fetal wounds, and the unique fetal fibroblast phenotype characterized by increased HA production and increased migration and invasion capabilities (1). Compared to this benchmark, fetuses begin to permanently shift towards a phenotype more prone to scarring in late gestation, which persists throughout the rest of the life span. This coincides with increased expression of Engrailed-1 (EN1) and CD26+ fibroblasts in the late gestation and postnatal dermis (2). Rinkevich et al. identified these CD26+ fibroblasts as the primary drivers of pro-fibrotic remodeling during wound healing, including in post parturition wounds. However, not all midgestation fetal wounds heal regeneratively, and larger wounds of critical defect size made in the midgestation fetus heal with the formation of a scar at the same gestation, while smaller wounds heal without scar formation (3). The underlying mechanisms that govern the fetal regenerative healing and its perturbation in large wounds remain incompletely understood.

(HA) is an extracellular matrix (ECM) component key to the wound healing process. HA alters the availability and activity of various growth factors in a wound, as well as regulates the inflammatory and angiogenic responses to injury. The molecular weight (MW) of HA alters its signaling effects. Low molecular weight (LMW) HA exerts

proinflammatory effects, while high molecular weight (HMW) HA promotes anti-inflammatory responses (4-7). The anti-inflammatory effects of HMW-HA are mediated through CD44, the primary cell-surface receptor for HA. HA expression in the wounds is governed by its production and degradation enzymes, including synthesis enzymes hyaluronan synthase (HAS) 1-3 and degradation enzymes hyaluronidase (HYAL) 1-2 and KIAA1199, a HA binding protein involved in HA depolymerization (8, 9). Importantly, HAS1-2 are associated with HMW-HA production (2x10^5 – 2x10^6 kDa), while HAS3 is associated with the production of lower molecular weight (1x10^5 – 1x10^6 kDa) HA. HMW-HA stability is critical to sustain and promote its role in regenerative wound healing, as its catabolism in the wounds generates LMW-HA that will promote pro-inflammatory and pro-fibrotic responses (10). Thus, the balance of HA-forming enzymes and HA-degrading enzymes in the wounds impacts the final balance of HMW to LMW HA in the wound microenvironment, determining how the wound will heal.

Dermal fibroblasts drive both the synthesis and remodeling of the wound ECM (1). Thus, dermal fibroblasts can influence the fibrotic outcome of a healing wound. The phenotype and activity of mid-gestational fetal fibroblasts (FFB) differs significantly from the phenotype of adult fibroblasts (AFB). Notably, these phenotypic differences include their migratory potentials, rate of proliferation and differentiation, cytokine production, and ECM synthesis (11). More specifically, we have shown that FFB characteristically secrete more HA than AFB, and this secreted HA forms a pericellular coat around the FFB (12). This pericellular coat of HA both regulates the metabolic rates of FFB and facilitates the migration and invasion of FFB into wounds. Importantly, inhibiting HA production in FFB using 4-MU attenuated their levels of migration and invasion to levels

similar to that of AFB (12). These differences may partially explain why mid-gestation mammalian fetuses heal regeneratively, whereas similar wounds on a post-natal individual produces fibrosis and heal with scar.

Research demonstrates that wound tension alters the expression of fibrogenic markers in fibroblasts. Fibroblasts in a wound are subjected to changes in mechanical force balance during wound healing, and thereby mount an increase in their tensile forces to facilitate wound closure by bringing in the wound margins together (13, 14). Mechanically stressed fibroblasts differentiate into the specialized myofibroblast phenotype, characterized by expression of -smooth muscle actin and formation of prominent stress fibers (15, 16). In practice, this means tension on a wound should be minimized to lower the risk of scarring. Indeed, offloading tension on adult wounds significantly reduces scarring, relative to non- stress-shielded wounds (17). Previous studies have shown that the resting tension in fetal skin is negligible and significantly lower than in adult skin (18). The lower resting tension of fetal skin acts much like a stress-shield and is perhaps linked to regenerative healing of moderate sized wounds. However, increasing wound defect size in the fetus shifts the wound healing process from a regenerative to a scarring phenotype through unknown mechanisms. We posit that increasing wound size in fetal wounds increases the mechanical forces on the fibroblasts that are needed to close the wound. However, the fetal fibroblast responses to increase in mechanical tension is not known.

In sum, evidence shows that both the balance of HMWHA and LMWHA within a wound and the tension on a wound can individually determine the outcome of a healing wound. However, it is currently not well understood how increases in mechanical loads

during wound healing alter fetal fibroblast HA behavior. Thus, we sought to determine how mechanical tension influences the balance of HA metabolism (synthesis and degradation) and the fibrogenic potential and migration of fetal fibroblasts as compared to adult fibroblasts. We hypothesize that increase in mechanical tension by increasing strain alters HA metabolism in FFB, with tension driving LMW-HA and profibrotic responses in FFB.

METHODS

Cell isolation and culture

All protocols were approved by the Baylor College of Medicine Institutional Animal Care and Use Committee. Primary fetal murine dermal fibroblasts (FFB) were isolated from mid-gestation age fetuses (E14.5) from control C57BL/6J (Strain numbers 000664, Jackson Laboratories, BarHarbor, ME) using standard isolation protocols. Primary adult murine dermal fibroblasts (AFB) were obtained from control C57BL/6J adult mice (8–12weeks). Skin from bilateral flanks was excised and used for cell isolation. Cells were plated in BD Falcone cell culture flasks (BDBiosciences, Bedford, MA) without any additional surface coating, and the fibroblast culture was maintained in Dulbecco's Modified Eagle's media with GlutaMAX 1mg/ml (DMEM) (GIBCO, Carlsbad, CA) supplemented with 10% bovine growth serum (BGS) (Hyclone, Logan, UT), 1% sodium pyruvate, penicillin 100 units, streptomycin 100 µg and amphotericinB 0.25 µg (Invitrogen,Carlsbad, CA),and maintained in a humidified chamber at 37°C with 5% CO2. Cells between passages 3–8 were used for experiments.

Fibroblast cultures on flexible membranes

A mechanical strain device (FX3000, Flexcell International Corp.) was used to apply radial and circumferential cellular strain to murine FFB and AFB to determine the effect of mechanical tension on their HA and fibrotic phenotype. 50,000 cells were seeded as monolayers on collagen I-coated silicone membranes in 6-well plates (BioFlex Culture Plate, Flexcell Corp.) and allowed to attach to membranes overnight. Cells were cultured as stated above. Six planar cylinders (25 mm diameter) served as loading posts for the culture plates which were centered beneath each 35-mm well. By application of vacuum, cyclic equibiaxial strain at 10% was applied to the fibroblast monolayer, which underwent static/tonic deformation for up to 1, 3, 6, 12 and 24h. Before applying the mechanical loading, culture medium was exchanged, and 3 ml of fresh Dulbecco's modified Eagle's medium containing 10% BGS was added. Cells cultured in identical conditions on the flexible membranes without applied tension in the same incubator served as controls.

Particle Exclusion Assay for Pericellular Matrix Analysis

Pericellular matrix (PCM) area was measured using a particle exclusion assay as described previously(19). Briefly, glutaraldehyde-stabilized sheep red blood cells were added to FFB and AFB cultured under static or tension conditions after 24h and the exclusion of fixed red blood cells was used to visualize fibroblast pericellular coats. Cells were rinsed in PBS, and 1ml glutaraldehyde-stabilized sheep erythrocytes (1×10^8 cells/ml; Intercell Technologies, Jupiter, FL, USA) were added to each well and allowed to settle for 10 min. Individual cells were imaged under phase contrast at ×20 magnification with an Axiovert 100M inverted phase contrast microscope (Carl Zeiss,

Thornwood, NY, USA), which showed the outline of the cell body and the outline of the HA coat as a halo around the cells bounded by the red blood cells. Images of randomly selected cells (20–30 cells/group) from each group were analyzed with ImageJ software, and the PCM ratio was reported as the ratio the area of the PCM plus the cell body area to the cell body area alone.

Immunocytochemistry

After 6h under static or tension conditions, cells were fixed with 4% paraformaldehyde for 10 min at room temperature. Cells were then permeabilized with 0.01% Triton-X100 when looking for intracellular targets only and blocked with 1% BSA in PBS for 1 h at room temperature. Primary antibodies were diluted in 1% BSA and allowed to bind overnight at 4C. Cells were incubated with anti-CD26, (rabbit mAb; Abcam), anti-a-SMA, (rabbit mAb; Abcam) then detected with an appropriate fluorescent secondary antibody for 1 h at room temperature. For detection of CD44 and HA, cells were not permeabilized, and incubated with anti-CD44 (rabbit mAb; Abcam), HABP (rabbit mAb; Abcam), Phalloidin, (AF 488 conjugated; Life Technologies) samples were counterstained with DAPI before imaging with a Leica DMi8 fluorescent microscope.

HA Extraction and Gel electrophoresis

Cell culture supernatants were collected after treatment, and 10% volume of Proteinase K (Invitrogen, 1 mg/ml with SDS at 0.01%) was added and incubated at 60 °C for 4 hours to digest the proteins. 4ml pre-chilled (-20 °C) 200 proof ethanol was added and incubated overnight at -20 °C. Samples were centrifuged at 14,000g for 10 minutes at room temperature (RT). The pellets were washed with 4ml 75% EtOH and vortexed

followed by centrifugation at 14,000g for 10 minutes. The supernatant was completely discarded and the pellet was air dried at RT for 20 minutes. 100µl of 100 mM ammonium acetate (Sigma-Aldrich) was added to re-suspend the pellet, and the samples were heated at 100 °C for 5min to inactivate Proteinase K. Samples were then chilled on ice for 5 min, followed by addition of 1 µl of Benzonase (EMD Millipore), and incubation overnight at 37 °C to digest nucleic acids. Samples were boiled for 5 minutes to inactivate enzymes. We then added 200 µl cold 200 proof ethanol to half of the suspension and incubated overnight at -20 °C, followed by centrifugation at 14,000 g for 10 minutes at RT. Supernatant was discarded and the pellet was washed with 1 ml cold 75% ethanol and centrifuged as before and air dried for 20 min. The pellet was then re-suspended in 10 µl of 10 M formamide at 4 °C overnight. The other half sample was used to validate HA, by digestion with hyaluronidase, and using it as a negative control for gel electrophoresis. In order to do this, HA pellet was re-suspended in 10 µl 100 mM ammonium acetate (pH 7.0). Then 1 µl Streptomyces hyaluronidase (Millipore Sigma) was added and incubated at 37 °C overnight, followed by heat inactivation of the enzymes by placing the sample in boiling water bath for 5 minutes.

For HA gel electrophoresis, 1% agarose gel was cast and used (SeaKem HGT Agarose, Cambrex). In 1x TAE buffer, 2 µl of the sample loading solution (0.2% bromophenol blue in 10 M formamide) was mixed to each 10 µl sample. Hyaluronan standards (Select-HA^{TM}, Hyalose) were prepared similarly. Prior to loading, HA concentration was confirmed with Hyaluronic Acid (HA) test kit (Corgenix Specialists in ELISA Diagnostic Technology) according manufacturer's instruction. Samples and standards were loaded, and the gel was run at 100 V until the tracking dye has migrated

about 75% of the length of the gel. Gels were equilibrated with 30% ethanol then stained with Stains-All (Sigma-Aldrich, E9379) solution overnight in the dark. Gels were washed and equilibrated with water before exposure to light to destain. Gels were exposed until desired destaining was achieved and then promptly imaged.

Scratch Wound Assay

FFB were seeded in 6-well flexible membrane culture plates similar to above experiments with gelatin coating at a density of 1.0×10^6 cells per well in 3 ml DMEM containing 10%BGS and allowed to adhere overnight. The media was removed, and cells were then serum starved in DMEM containing only 2%BGS for 24 hours prior to the treatment. A scratch defect was created in the cell monolayer along the diameter in each group using a sterile pipette tip (20–200 µl tip). Five points were marked and defined along the scratch defect, which were used as reference points to capture photographic images to trace defect closure at multiple time points. Cells were subjected to 10% strain similar to above experiments on the Flexcell apparatus for a total of 6 hours. Plates were removed from Flexcell system and cultured in the incubator under normal static conditions. Images of the scratch were taken immediately after the 6-hour tension period and every 12 hours thereafter. Phase contrast imaging with an Axiovert100M inverted microscope (Carl Zeiss, Thornwood, NY) was used to obtain 4ximages. The unfilled scratch defect area was measured at each reference point per well, averaged over 5 fields per well. Data was presented as the percentage by which the scratch area has decreased at a given time point for each treatment as compared to the original defect (at 0 hours).

Real-time quantitative PCR and PCR Fibrosis Array

After completion of the mechanical loading cycle for 1, 3, 6, 12 or 24h, culture supernatants were collected and stored away in -80C with protease inhibitor cocktail (Sigma). Cell monolayers were washed in PBS and lysis buffer was added to the wells in both tension and static control cultures. Lysates were vortexed and frozen at -80^{0}C. Total RNA was isolated by using the PureLink^{TM} RNA Micro Kit (Invitrogen Cat# 12 183-016). After concentration and purity determination, cDNA was reverse-transcribed from 500 ng of RNA using the RT^2 first strand kit (Cat# 330404) following manufacturers protocols (Applied Biosystems, Foster City, CA, USA) and amplified by quantitative PCR using forward and reverse primers (Integrated DNA Technologies, Coralville, IA, USA) and Power SYBR Green PCR Master Mix in a StepOne-Plus Real-Time PCR system(Applied Biosystems, Foster City, CA, USA). Mouse Gapdh gene expression was used to normalize the amount of the amplified products. Relative expression values were calculated by using the ΔΔCt method (20). Primer sequences are listed in **Table 1**, those purchased from Bio Rad are indicated.

We also used the RT^2 Profiler PCR Array mouse fibrosis (cat. #PAMM 120-ZE-4) kits from Qiagen to detect the expression of 84 fibrosis-related genes. This assay uses the same cDNA made with RT2 first strand kit (cat. #330404) and RT2 SYBR Green qPCR Mastermix (Qiagen cat. #330501). Bio-Rad CFX 384 real-time system and Bio-Rad CFX manager software were used for real-time PCR. Data were analyzed by Qiagen RT2 Profiler PCR Array data analysis software. Principal Component Analysis (PCA) was performed with Orange software (https://orange.biolab.si). Gapdh was used

as a housekeeping gene, and ΔCT values for the genes were analyzed with the above Orange program.

Statistical Analysis

Statistical significance of the data was evaluated using analysis of variance (ANOVA), followed by post-hoc tests (Tukey) and Student's t-test when appropriate. MS-Excel (Microsoft, Redmond, WA) was used for the purpose.

RESULTS

Tension decreases PCM surrounding fetal fibroblasts

We have previously shown that the FFB produce a characteristic HA-comprising PCM coat on the cell surface as compared to AFB(19). When HA was inhibited in FFB, their PCM coats were reduced and resembled those in AFB, both in the size of the coat and their SEM structure (11, 19). We therefore used PCM analysis first to interrogate the impact of tension on extracellular matrix production of FFB, illustrated in **Figure 1a**. Baseline PCM measurements demonstrate significantly decreased PCM surrounding AFB when compared to FFB (1.84 ± 0.08 PCM area/Cell area vs. 2.78 ±0.14 PCM area/Cell area, $P<0.01$), which is consistent with prior findings. FFB cultured under tension showed a reduced PCM area as compared to FFB under static conditions (1.98 ± 0.15 PCM area/Cell area vs. 2.78 ±0.14 PCM area/Cell area, $P<0.01$), and after 24 hours of tension resembles PCM of AFB grown in static conditions (1.98 ± 0.15 PCM area/Cell area vs. 1.84 ± 0.08 PCM area/Cell area, NS) (**Figure 1b**).

HA Metabolism balance shifts toward LMW-HA with tension

Knowing that the majority of the PCM surrounding fibroblasts consists of HA, we sought to understand how tension impacts regulation of HA metabolism to further explain the observation that tension reduces the PCM coats of FFB. Gene expression profiles of HA metabolism (HAS1-3, KIAA1199, and HYAL1-2) at intervals of 0, 1, 3, 6, and 12 hours after the application of tension were measured by qPCR (**Figure 2**). FFB and AFB demonstrate significantly different intrinsic HA metabolism profiles at baseline, with significantly lower HAS1 (1.004 vs 6.8 fold regulation, $p<0.05$), HAS2 (1,003 vs 1.7 fold regulation, $p<0.05$), KIAA1199 (1.006 vs 17.5 fold regulation, $p<0.05$), HYAL 1 (1.02 vs 4.4 fold regulation, $p<0.05$), and HYAL 2 (1.003 vs 1.4 fold regulation, $p<0.05$) expression in FFB (**Figure 2a**), suggesting that at baseline, AFB has higher PCM turnover. Tension had differential effects on gene regulation of HA metabolism between AFB and FFB (**Figure 2b-g**). There was decreased HAS2 expression in both AFB and FFB with tension. KIAA1199 expression in FFB increased over time but not AFB ($p<0.001$). HAS3 expression was appeared to remain steady in AFB over time with tension, while increasing in FFB with tension. HYAL1 expression decreased over time in both FFB and AFB under tension with AFB showing the highest expression at 6h. In sum, tension resulted in an increase in HAS1, HAS3, and HYAL1 expression in FFB, and decreased HAS2 but increased HYAL1 for AFB under tension (**Table 2**).

As these overall changes in HA metabolism in AFB and FFB under tension indicate a possible shift towards a profile consistent with a lower molecular weight HA, we sought to determine the effect of the tension on HA molecular weight patterns using gel electrophoresis. Images of the gels (**Figure 2h**) demonstrate that the HMW-HA

(>1x10^6 kDa) noted in the static FFB and at 6 hours after tension is by and large abrogated after 24 hours of tension, once again resembling the molecular weight of HA produced by static AFB and at both 6 and 24 hours of tension.

Tension leads to organization of cytoskeletal elements in fetal fibroblasts

As the changes in the PCM coats of the FFB may affect the cell's interaction with its microenvironment and thereby drive potential changes in its internal cytoskeletal organization, we sought to understand the effect of the tension on organization of the cytoskeletal cell elements. AFB and FFB were stained for filamentous actin using fluorophore-conjugated phalloidin after 6 hours of static and tension conditions. Qualitatively, at the baseline, F-actin (**Figure 3**) in static AFB appear to have large filaments running in a parallel orientation when compared to a disoriented "bird nest" appearance composed of shorter cords in static FFB. Following 6 hours of tension, F-actin in FFB shifts into a more parallel orientation of larger cords, akin to AFB under both the static conditions and after 6 hours of tension.

Staining for aSMA was in congruence with these findings. AFB and FFB were stained with antibodies against-aSMA after 24 hours of static and tension conditions. At baseline in static culture, there appears to be more aSMA in AFB as compared to FFB (**Figure 4a**). aSMA fibers in static AFB appear to be in a parallel orientation when compared to no specific orientation in static FFB. Following 6 hours of tension, there appears to be more aSMA in AFB, and while there does not appear to be an increase in aSMA expression level in FFB, the fibers appear organized in the same parallel fashion as AFB. Expression of aSMA by AFB was confirmed to be significantly increased at

specific timepoints of tension (1, 3, 6, and 12hr) when compared to static AFB using qRT-PCR analysis, while no significant change in gene expression of aSMA was seen in FFB when exposed to tension at these timepoints (**Figure 4b**).

Tension differentially increases fibrogenic potential in both adult and fetal fibroblasts

Our data thus far suggest that tension induces changes in HA expression and molecular weight, along with changes in the ECM organization and stress filaments, which could also lead to subsequent changes in the functional fibrotic phenotype of the FFB. To begin to understand how tension effects the fibrotic phenotype of FFB and AFB, we sought to evaluate CD26, a cell surface marker that has been shown to be positively correlated with fibroblast fibrogenic propensity (2). **Figure 6a** demonstrates representative ICC for CD26. Qualitative analysis suggests that the amount of CD26 on cell membrane of FFB increases after 24 hours of tension when compared to static condition, whereas CD26 content of AFB appears to remain constant with tension. Analysis of CD26 gene expression revealed an upregulation in the FFB under tension at early time points versus static conditions (4.5 ± 1.2 vs 1.1 ± 0.5, $P<0.01$), with no significant change in expression over time in AFB (**Figure 6b**). These results suggest that the 10% strain is inducing gene expression that transitions the cells to fibrogenic a phenotype in the FFB, shifting the FFB to be similar to its adult counterpart AFB.

To further characterize the effect of tension on fibrotic gene changes in FFB and AFB, we next utilized a PCR-based 84 gene fibrosis array. Principle Component Analysis (PCA) of the top 25 differentially altered genes ranked by their effect on overall fibrotic phenotype are plotted in **Figure 6a**. When AFB and FFB are exposed to tension, in

multi-dimensional sampling analysis, FFB tension is more similar in phenotype to AFB static and AFB tension compared to FFB static, indicating a similar effect on fibrotic gene regulation (**Figure 6b**). **Figure 6c** shows Venn diagrams illustrating the proportion of common or unique up- or downregulated of fibrotic genes seen between AFB and FFB exposed to tension. We found 17 genes to be upregulated with tension (5 of them exclusively in FFB, 4 exclusively in AFB, and 8 upregulated in both FFB and AFB). We found 28 genes to be downregulated with tension (13 of them exclusively in FFB, 8 exclusively in AFB, and 7 downregulated in both FFB and AFB). The specific up- or down- regulation of gene expression illustrated in Figure 6b are listed in **Table 3** (upregulated) and **Table 4** (downregulated). Many genes involved in inflammation (Interleukins 1a, 5, and 13) and inflammatory signal transduction (C-jun) were upregulated by tension in AFB and FFB. Itga2 and Itgb3 are genes involved in cell adhesion and were downregulated by tension in both AFB and FFB. Some genes involved in the TGF-ß family of inflammatory signal transduction (Smad6 and Thbs1) were downregulated by tension in both AFB and FFB. A gene involved in ECM remodeling (Mmp13) was exclusively upregulated in FFB exposed to tension.

Tension reduces number of fetal fibroblasts adherent to culture plate over time

While performing ICC for aSMA and phalloidin, we noticed that the cellular density of FFB appeared to decrease after 24hr of tension, thus we sought to objectively measure the absolute change in cell number with mechanical tension. Cells were subjected to tonic stretch for up to 24hr and the morphology and cell attachment were observed (**Figure 7a-j**). Qualitatively, adult fibroblasts tolerated 24hr of tension and appeared

normal in cell morphology, with minimal visual change in cell density after 24hr of exposure to tension. In contrast, after even 6hr of exposure to tension, FFB appeared rounded with disrupted attachment to the culture plate, and by 24hr, the absolute number of FFB adhered to the culture plate had decreased remarkably. Quantification of both AFB and FFB confirmed these observations (**Figure 1k**). Results are shown as a percent change from the control seeding density at 0hr. For AFB, there was minimal percent change in cell density throughout the 24hr period, with a slight increase (from 100% density to 109%), indicating some degree of continued proliferation despite tension conditions. In contrast, there was a marked decrease FFB cell density, with a mean density 100% at 0hr, 76% at 3hr, 47% at 6hr, 19% at 12hr, and finally 10% by 24hr ($P<0.001$).

Tension alters functional properties of FFB *in vitro*

As previous groups have shown the HA receptor CD44 interacts with an HA-rich environment to mediate cell migration(21), and CD44 expression is regulated in part by the stiffness of the cellular environment (22), we next explored changes in functional measures of FFB exposed to tension. We focused on the 6-hour time point, as roughly half of the initial FFB remained at this time point, and gene expression at this point would still reflect a significant proportion of the FFB in response to tension. **Figure 8a-d** demonstrates staining for HABP and CD44 in FFB after 6-hours of tension. The morphology of cells was similar to previous characterizations, with more rounded cells after tension. HA appears to form long thin tendrils between cells after tension. CD44 expression is diffusely expressed throughout the static cells, and transition to discrete

islands of positivity after exposed to tension. Quantitatively, there is no change in the expression of CD44 over the course of 12h of tension (**Figure 8e**). Knowing that CD44 expression and CD44 mediated cell migration can be affected by substrate stiffness, we sought to demonstrate how tension affects the migration of FFB. Using a scratch wound assay (**Figure 8f**), we demonstrated that FFB exposed to tension demonstrated decreased wound closure in this model.

DISCUSSION

Fundamentally, fetal wounds heal regeneratively while wound healing in adults is marked by scarring. In both, the wound repair process is intricate and influenced by a number of intrinsic and extrinsic factors. This work is aimed at investigating the intrinsic differences in response to tension between fetal and adult fibroblasts, so as to further understand and potentially recapitulate the fetal regenerative healing phenotype in postnatal wounds. Scarring is a disease process that causes significant morbidity and mortality, and though currently available anti-scarring therapies make up a multi-billion-dollar industry, none have been able to successfully reverse the scarring phenotype (23, 24). Understanding the mechanisms behind the fetal regenerative phenotype allows us to pursue anti-scarring therapeutics based upon a biological process which we know is naturally feasible.

In this work, we investigated the effect of tension on fetal fibroblasts, which naturally reside in an environment with little mechanical stress, by measuring markers of fibroblast phenotype. We report an intrinsic characteristic of FFB to respond to tension by decreasing synthesis of HMW-HA, thus reducing their HA rich PCM in a way which resembles their adult counterparts. HA is a major structural and functional component of

the extracellular matrix and plays an essential role in every organ system of the body such as organ development, inflammation, and cell migration (4). FFB proliferate and migrate more effectively as compared to their postnatal counterparts because of the hydrated microenvironment made possible by HA rich ECM (19). We also explored the balance of HA homeostasis in AFB and FFB in static and tension conditions. To this end, we measured the expression levels of hyaluronan synthases, HAS1, HAS2, HAS3 and hyaluronanidases, HYAL1, HYAL 2. We also assessed expression levels of KIA1199, a gene involved in HA catabolism that plays a role in HA binding and depolymerization. We found that fetal and adult fibroblasts have inherently different HA metabolism profiles with higher HAS2 and lower KIAA1199 expression in FFB. There is no significant difference in HAS2 and KIAA1199 levels on application of tension in FFB, however, expression of both are decreased in adult fibroblasts at baseline. Tension increased expression of HAS1 and HAS3 in both FFB and AFB. Further, we also found that HYAL1 levels are increased in FFB and AFB under tension, whereas HYAL2 expression remain unchanged. Increased hyaluronidase activity is characteristic of adult and late gestational fibrotic wound healing (25). This change in the homeostatic balance of HA metabolism corroborates our findings of overall decreased HMW-HA production by FFB in response to tension. This data correlates well with known evidence of elevated HA synthesis and sustained HA deposition in fetal wounds at baseline (26). It has been proposed that prolonged presence of HA in fetal wounds may provide the mesenchymal signal for healing by regeneration rather than by scarring and fibrosis (27).

Next, we sought to determine if tension confers a profibrotic phenotype to fetal fibroblasts. CD26, a member of the dipeptidyl peptidase family, was recently elucidated to be a marker for fibroblast lineage responsible for the tissue remodeling during physiological wound healing (3). Our data demonstrates that CD26 levels were found to be upregulated in FFB only under tension, while AFB have elevated CD26 levels both under static conditions as well as tension. We also assessed the levels of α-SMA, a marker of myofibroblasts that are characteristic of adult wound healing. α-SMA is absent in fetal wound healing and its appearance coincides with the onset of scar formation seen in later gestation (28). While tension had no effect on α-SMA expression in FFB, qualitative analysis of α-SMA organization did demonstrate that the intracellular α-SMA in FFB grown under tension did result in parallel cords that spanned the entire cell, resembling the structure in AFB. The same observations were seen with intracellular F-actin of FFB, transitioning from a “bird’s nest” appearance of disorganized fibers to parallel bundles that span the entire cells, akin to AFB at baseline. These organized bundles represent stress fibers, which consist of numerous actin filaments, and can produce contractile forces similar to myofibrils of muscle cells, though lacking the same organization (29). While chemical signaling pathways are known to regulate the formation of stress fibers, the ultrastructure of these fibers are dynamic, and their formation and orientation can be influenced by intra- and extracellular mechanical forces (30). While the observation that stress induces organization of stress fibers in FFB to a similar appearance of AFB does not necessarily signal a change to a more fibrotic phenotype, it is known that the function of stress fibers are, in part, determined by their ultrastructure, and range from contraction to transcriptional regulation of genes

involved in matrix reorganization and locomotion (31). Though it is beyond the scope of this paper to characterize the exact ultrastructure and function of the stress fibers seen, the alterations seen in fiber organization are notable as support of our hypothesis that tension induces functional phenotypic changes in FFB that make them similar to AFB.

Our finding that tension reduces the number of FFB adherent to the culture plate poses an issue that limits the interpretation of our data. We see an increase in CD26 expression in FFB as a result of tension, however, the experimental design does not allow us to determine if only a CD26 positive lineage is able to tolerate the tension, or if tension is inducing CD26 in all cells, and some of those cells happen to detach from the culture plate. In the context of fetal wound healing, and knowing that CD26 is a marker of a pro-fibrotic fibroblast lineage, it stands to reason that the mechanical force generated within a larger wound in the fetus may create an environment in which only CD26-positive fibroblasts can tolerate. Thus, the scarring seen from large fetal dermal wounds can be attributed to a lineage of fibroblasts that can both tolerate tension and has a fibrotic phenotype, while the lineages of anti-fibrotic fibroblasts apoptose or are unable to migrate into the wound. A closer look at the time course of CD26 expression in FFB under tension reveals that CD26 is most upregulated at 1 and 3 hours of tension, relatively early in the time course of the experiment. At these time points, there has not been as dramatic a decrease in FFB cell numbers (24% decrease at 3h). We posit that tension does trigger increased expression of CD26, but only those cells that are further down the path of differentiation into CD26 positive cells are able to confer the fibrotic phenotype that allows for tolerance of the tension. Therefore, further study is needed to address this dilemma.

Moving forward, the fate of specific FFB cells needs to be ascertained, whether they are simply detaching from the plate and are unable to withstand the tension, or if they are truly dying via apoptosis mechanisms.

In summary, we have presented here an explanation for the scarring seen in fetal wounds of greater size. The larger size of the wound would result in increased tension on fibroblasts, and through mechanisms presented above, result in a profibrotic phenotypic change of FFB to that of their adult counterparts.

ACKNOWLEDGMENTS

This research was supported by the 3M Foundation Award provided by the Wound Healing Society.

AUTHOR CONTRIBUTIONS

SB, MF, XY designed the experiments. UMP, NT, AB, DC, HS, AK, MMF, SB performed bench and animal-related experimental work. UMP, WDS, MMF, SB analyzed data. UMP, WDS, MF, SB wrote the manuscript. SB, XY, MMF provided scientific comments for the study and significant content revisions to the manuscript. All authors have reviewed and approve the final version of the manuscript.

LIST OF ABBREVIATIONS

HA, Hyaluronan; EN1, Engrailed-1; ECM, Extracellular Matrix; MW, Molecular Weight; LMW-HA, Low Molecular Weight Hyaluronan; HMW-HA, High Molecular Weight Hyaluronan; HAS, Hyaluronan Synthase; HYAL, Hyaluronidase; FFB, Fetal Fibroblasts; AFB, Adult Fibroblasts

Table 1.

Primer sequences for quantitative PCR validation

Oligonucleotide	Sequence, 5′–3′ F	Sequence, 5′–3′ R
Mo Has1	CATGGGCTATGCTACCAAGT	TCAACCAACGAAGGAAGGA
Mo Has2	[Bio Rad Primer]	
Mo Has3	CAGTGGACTACATCCAGAGGTG	ACTCGAAGCATCTCAATGGT
Mo Hyal1	[Bio Rad Primer]	
Mo Hyal2	TCTTCACGCGTCCCACATA	GCACTCTCACCGATGGTAGA
Mo CD44	TTCATCCCAACGCTATCTGTG	CGAAGGAATTGGGTAGGTCTG
Mo CD26	GTCATAGGATCACATCGACAGG	ACTGGGCATAAGCTAGAAACG
Mo KIAA1199	CTCAGCTGAAGACAAAAGAC	ATTCCGAAGGTGGAAGAAG
Mo aSMA	[Bio Rad Primer]	
Mo GAPDH	GCTGGAGAAGGTTTGTGCG	AGTGATTCTCAAAGTCTTGGTAGGC

F, forward; R, reverse.

Table 2.

Overall changes in regulation of HA metabolism in adult and fetal fibroblasts after tension.

	AFB + Tension	**FFB + Tension**
HAS1 (HMW)	↑	↑
HAS2 (HMW)	↓	↓
HAS3 (LMW)	**---**	↑
HYAL1	↑	↑
HYAL2	**---**	**---**
KIAA1199	**---**	↓
HA PROFILE	**LMW HA**	**LMW HA**

Table 3.

List of genes that are commonly and uniquely upregulated in adult and fetal fibroblasts.

Upregulated genes		Fold Regulation	
Gene Symbol	Gene Name	AFB	FFB
Common			
Fasl	Fas Ligand	14.26	7.45
IL5	Interleukin 5	9.74	2.87
IL13	Interleukin 13	3.22	4.61
IL10	Interleukin 10	2.88	32.46
Jun	c-Jun	2.81	2.01
IL1a	Interleukin 1a	2.34	2.19
Only in AFB			
Timp4	TIMP metallopeptidase inhibitor 4	8.09	
Agt	angiotensinogen	5.57	
Only in FFB			
Mmp13	matrix metalloproteinase 3		8.95
IL4	Interleukin 4		6.01
Cxcr4	CXC motif chemokine receptor 4		4.67
Bmp7	bone morphogenetic protein 7		2.56

Table 4.

List of genes that are commonly and uniquely downregulated in adult and fetal fibroblasts.

Downregulated genes		Fold Regulation	
Gene Symbol	Gene Name	AFB	FFB
Common			
Ccl11	eotaxin 1	-4.76	-2.59
Itga2	integrin subunit alpha 2	-3.18	-1.56
Itgb3	integrin subunit beta 3	-3.14	-1.86
Smad6	Smad family member 6	-2.76	-2.90
Hgf	hepatocyte growth factor	-2.16	-2.51
Thbs1	thrombospondin 1	-1.77	-2.28
Col3a1	Collagen type 3a	-1.70	-2.13
Only in AFB			
Cxcr4	CXC motif chemokine receptor 4	-4.19	
Bmp7	bone morphogenetic protein 7	-2.44	
Dcn	decorin	-2.35	
Only in FFB			
Pdgfb	platelet-derived growth factor subunit B		-10.29
Itgb8	integrin subunit beta 8		-3.15
Agt	angiotensinogen		-2.85
Tgfb3	transforming growth factor beta 3		-2.34

Itga1	integrin subunit alpha 1	-2.08
Serpine1	serpin family e	-2.08
Egf	epidermal growth factor	-2.00

References

1. **Lorenz HP, Lin RY, Longaker MT, Whitby DJ, and Adzick NS**. The fetal fibroblast: the effector cell of scarless fetal skin repair. *Plast Reconstr Surg* 96: 1251-1259; discussion 1260-1251, 1995.

2. **Rinkevich Y, Walmsley GG, Hu MS, Maan ZN, Newman AM, Drukker M, Januszyk M, Krampitz GW, Gurtner GC, Lorenz HP, Weissman IL, and Longaker MT**. Skin fibrosis. Identification and isolation of a dermal lineage with intrinsic fibrogenic potential. *Science* 348: aaa2151, 2015.

3. **Morris MW, Jr., Allukian M, 3rd, Herdrich BJ, Caskey RC, Zgheib C, Xu J, Dorsett-Martin W, Mitchell ME, and Liechty KW**. Modulation of the inflammatory response by increasing fetal wound size or interleukin-10 overexpression determines wound phenotype and scar formation. *Wound Repair Regen* 22: 406-414, 2014.

4. **Garantziotis S, and Savani RC**. Hyaluronan biology: A complex balancing act of structure, function, location and context. *Matrix Biol* 78-79: 1-10, 2019.

5. **Shi Q, Zhao L, Xu C, Zhang L, and Zhao H**. High Molecular Weight Hyaluronan Suppresses Macrophage M1 Polarization and Enhances IL-10 Production in PM2.5-Induced Lung Inflammation. *Molecules* 24: 2019.

6. **Tamoto K, Nochi H, Tada M, Shimada S, Mori Y, Kataoka S, Suzuki Y, and Nakamura T**. High-molecular-weight hyaluronic acids inhibit chemotaxis and phagocytosis but not lysosomal enzyme release induced by receptor-mediated stimulations in guinea pig phagocytes. *Microbiol Immunol* 38: 73-80, 1994.

7. **Soroosh A, Albeiroti S, West GA, Willard B, Fiocchi C, and de la Motte CA**. Crohn's Disease Fibroblasts Overproduce the Novel Protein KIAA1199 to Create

Proinflammatory Hyaluronan Fragments. *Cell Mol Gastroenterol Hepatol* 2: 358-368 e354, 2016.

8. **Weigel PH, and DeAngelis PL**. Hyaluronan synthases: a decade-plus of novel glycosyltransferases. *J Biol Chem* 282: 36777-36781, 2007.

9. **Kreil G**. Hyaluronidases--a group of neglected enzymes. *Protein Sci* 4: 1666-1669, 1995.

10. **Litwiniuk M, Krejner A, Speyrer MS, Gauto AR, and Grzela T**. Hyaluronic Acid in Inflammation and Tissue Regeneration. *Wounds* 28: 78-88, 2016.

11. **Balaji S, King A, Marsh E, LeSaint M, Bhattacharya SS, Han N, Dhamija Y, Ranjan R, Le LD, Bollyky PL, Crombleholme TM, and Keswani SG**. The role of interleukin-10 and hyaluronan in murine fetal fibroblast function in vitro: implications for recapitulating fetal regenerative wound healing. *PLoS One* 10: e0124302, 2015.

12. **King A, Balaji S, Le LD, Marsh E, Crombleholme TM, and Keswani SG**. Interleukin-10 regulates fetal extracellular matrix hyaluronan production. *J Pediatr Surg* 48: 1211-1217, 2013.

13. **Wong VW, Rustad KC, Akaishi S, Sorkin M, Glotzbach JP, Januszyk M, Nelson ER, Levi K, Paterno J, Vial IN, Kuang AA, Longaker MT, and Gurtner GC**. Focal adhesion kinase links mechanical force to skin fibrosis via inflammatory signaling. *Nat Med* 18: 148-152, 2011.

14. **Wilson CJ, Pearcy MJ, and Epari DR**. Mechanical tension as a driver of connective tissue growth in vitro. *Med Hypotheses* 83: 111-115, 2014.

15. **Goffin JM, Pittet P, Csucs G, Lussi JW, Meister JJ, and Hinz B**. Focal adhesion size controls tension-dependent recruitment of alpha-smooth muscle actin to stress fibers. *J Cell Biol* 172: 259-268, 2006.

16. **Leavitt T, Hu MS, Marshall CD, Barnes LA, Lorenz HP, and Longaker MT**. Scarless wound healing: finding the right cells and signals. *Cell Tissue Res* 365: 483-493, 2016.

17. **Gurtner GC, Dauskardt RH, Wong VW, Bhatt KA, Wu K, Vial IN, Padois K, Korman JM, and Longaker MT**. Improving cutaneous scar formation by controlling the mechanical environment: large animal and phase I studies. *Ann Surg* 254: 217-225, 2011.

18. **Parekh A, and Hebda PA**. The Contractile Phenotype of Dermal Fetal Fibroblasts in Scarless Wound Healing. *Curr Pathobiol Rep* 5: 271-277, 2017.

19. **Balaji S, Wang X, King A, Le LD, Bhattacharya SS, Moles CM, Butte MJ, de Jesus Perez VA, Liechty KW, Wight TN, Crombleholme TM, Bollyky PL, and Keswani SG**. Interleukin-10-mediated regenerative postnatal tissue repair is dependent on regulation of hyaluronan metabolism via fibroblast-specific STAT3 signaling. *Faseb j* 31: 868-881, 2017.

20. **Rao X, Huang X, Zhou Z, and Lin X**. An improvement of the 2ˆ(-delta delta CT) method for quantitative real-time polymerase chain reaction data analysis. *Biostat Bioinforma Biomath* 3: 71-85, 2013.

21. **Kim Y, and Kumar S**. CD44-mediated adhesion to hyaluronic acid contributes to mechanosensing and invasive motility. *Mol Cancer Res* 12: 1416-1429, 2014.

22. **Li S, Li C, Zhang Y, He X, Chen X, Zeng X, Liu F, Chen Y, and Chen J**. Targeting Mechanics-Induced Fibroblast Activation through CD44-RhoA-YAP Pathway Ameliorates Crystalline Silica-Induced Silicosis. *Theranostics* 9: 4993-5008, 2019.

23. **Moore AL, Marshall CD, Barnes LA, Murphy MP, Ransom RC, and Longaker MT**. Scarless wound healing: Transitioning from fetal research to regenerative healing. *Wiley Interdiscip Rev Dev Biol* 7: 2018.

24. **Monavarian M, Kader S, Moeinzadeh S, and Jabbari E**. Regenerative Scar-Free Skin Wound Healing. *Tissue Eng Part B Rev* 25: 294-311, 2019.

25. **West DC, Shaw DM, Lorenz P, Adzick NS, and Longaker MT**. Fibrotic healing of adult and late gestation fetal wounds correlates with increased hyaluronidase activity and removal of hyaluronan. *Int J Biochem Cell Biol* 29: 201-210, 1997.

26. **Chen WY, Grant ME, Schor AM, and Schor SL**. Differences between adult and foetal fibroblasts in the regulation of hyaluronate synthesis: correlation with migratory activity. *J Cell Sci* 94 (Pt 3): 577-584, 1989.

27. **Longaker MT, Harrison MR, Crombleholme TM, Langer JC, Decker M, Verrier ED, Spendlove R, and Stern R**. Studies in fetal wound healing: I. A factor in fetal serum that stimulates deposition of hyaluronic acid. *J Pediatr Surg* 24: 789-792, 1989.

28. **Cass DL, Sylvester KG, Yang EY, Crombleholme TM, and Adzick NS**. Myofibroblast persistence in fetal sheep wounds is associated with scar formation. *J Pediatr Surg* 32: 1017-1021; discussion 1021-1012, 1997.

29. **Naumanen P, Lappalainen P, and Hotulainen P**. Mechanisms of actin stress fibre assembly. *J Microsc* 231: 446-454, 2008.

30. **Hirata H, Tatsumi H, and Sokabe M**. Dynamics of actin filaments during tension-dependent formation of actin bundles. *Biochim Biophys Acta* 1770: 1115-1127, 2007.

31. **Sandbo N, and Dulin N**. Actin cytoskeleton in myofibroblast differentiation: ultrastructure defining form and driving function. *Transl Res* 158: 181-196, 2011.

Figure Legends

Figure 1: (A) Pericellular matrix coat (blue outline) secreted by adult and fetal fibroblast under static and 24h tension conditions. (B) At baseline, FFB has a large, HA-rich PCM. Under tension, FFB produced a much smaller PCM, more similar to the adult phenotype. *p<=0.05, **p<=0.01. Graphs are reported as mean ± SD.

Figure 2: Regulation of HA over the course of 24h of 10% static tension. (A) Shows the baseline differences of regulatory HA proteins at T0. Adult fibroblasts have much higher HA production and degradation than fetal fibroblasts under static conditions. Graph is reported as mean ± SD, *p<0.05. (B-D) Change of fold expression of hyaluronan synthase 1-3, (E) KIAA 1199, and (F-G) hyaluronidases 1 and 2. Each time point is expressed as mean or SD normalized to static conditions for each individual cell type at time 0. *p<=0.05, **p<=0.01, ***p<=0.001 compared to baseline expression in each cell line. Blue * indicates significance value for AFB, Red * indicates significance value for FFB. (H) Western blot gel indicating total hyaluronan expression in either adult fibroblasts (left) or fetal fibroblasts (right) in static and tension conditions at 6 and 24 hours. Adult fibroblasts, regardless of static or tension conditions, have an absence of HMW HA. In contrast, fetal cells at static 6h or with a short period of tension (6h), do express HMW HA, but by 24h tension, have decreased expression of HMW HA and are similar in expression to adult fibroblasts.

Figure 3: Immunocytochemistry fluorescent staining of F-actin (Phalloidin stain, green) in adult and fetal fibroblasts under static and 6h tension conditions. In adult cells under

either condition, orientation of F-actin fibers are linear and in parallel. In fetal cells under static conditions, F-actin filaments are disorganized and in no particular orientation. After 6h tension, F-actin fibers begin to resemble those of the adult cells and are in parallel orientation. Blue stain indicates DAPI staining for cell nucleus.

Figure 4: Immunocytochemistry fluorescent staining of alpha-SMA (red) in adult and fetal fibroblasts under static and 24h tension conditions. Alpha-SMA shows a similar pattern to F-actin, where in adult and fetal cells under static conditions, orientation of alpha-SMA fibers are parallel. After 24h tension, alpha-SMA fibers again begin to resemble those of the adult cells and are in parallel orientation and increased amounts than under static conditions. Blue stain indicates DAPI staining for cell nucleus. (b) Quantitative expression of a-SMA at 1, 3, 6, and 12 hours. Each time point is expressed as mean or SD normalized to static conditions at time 0. *p<=0.05, **p<=0.01, ***p<=0.001 compared to baseline expression in each cell line. Blue * indicates significance value for AFB, Red * indicates significance value for FFB.

Figure 5: Immunocytochemistry fluorescent staining of CD26 (red) in adult and fetal fibroblasts under static and 24h tension conditions. CD26 expression in fetal fibroblasts was upregulated by tension at early timepoints, suggesting that tension has a pro-fibrotic effect on fetal cells. Blue stain indicates DAPI staining for cell nucleus. (b) Quantitative fold regulation of CD26 at 1, 3, 6, and 12 hours. Each time point is expressed as mean or SD normalized to static conditions at time 0. *p<=0.05,

**p<=0.01, ***p<=0.001 compared to baseline expression in each cell line. Blue * indicates significance value for AFB, Red * indicates significance value for FFB.

Figure 6: (A) Principal Component Analysis of the top 25 fibrosis genes. (B) Multi-dimensional scaling analysis, which shows that FFB tension are now grouped in a similar manner to AFB static and tension, compared to FFB static. (C) Venn diagram showing the total number of fibrotic genes that were up- or downregulated in AFB and FFB cells.

Figure 7: Phase-contrast images of adults and fetal fibroblasts cells after 0 (A, F), 3 (B, G), 6 (C, H), 12 (D, I), and 24 (E, J) hours of 10% tonic tension. (K) Quantification of cells at each timepoint. Images were taken at 10X magnification, with 5 images taken per well in a 6 well plate (30 images quantified per timepoint). Each timepoint is expressed as a % of cells remaining from T0 ± SD. Streaks are due to vacuum grease residue that is utilized with the Flexcell machine.

Figure 8: This figure shows the functional phenotype of the fetal fibroblast. (A-B) Fluorescent staining with HA binding protein (HABP, green) and DAPI for cell nucleus (blue). In the FFB under static conditions, HA is diffusely expressed within the cell. After tension, these cells appear to have down-regulated HA, such that it is less expressed compared to static conditions, and when it is expressed, it forms cord-like structures between cells. (C-D) When these cells are co-labeled with CD44, we see more diffuse expression in CD44, and with tension, expression is more discrete and punctate. (E)

CD44 fold regulation changes over 12 hours of tension. Overall, expression did not change over time in fetal cells, while in adult cells, expression was upregulated at early timepoint of tension, at 2.8 ± 1.4-fold expression from baseline, and reduced to baseline levels by 12h. Each time point is expressed as mean or SD tension normalized to static in each condition. (F) Shows a scratch wound assay of the fetal fibroblast under static and tension conditions. After 6h of either tension or no tension, each condition was imaged every 12 hours until 84 hours. Under normal conditions, fetal fibroblasts achieved 89.1% wound closure by 84h, but after even 6h of tension, there was only 71.3% closure achieved by this same timepoint. Data reported as mean ± SD, n=5 sites/well, 3 wells/condition.

Figure 1

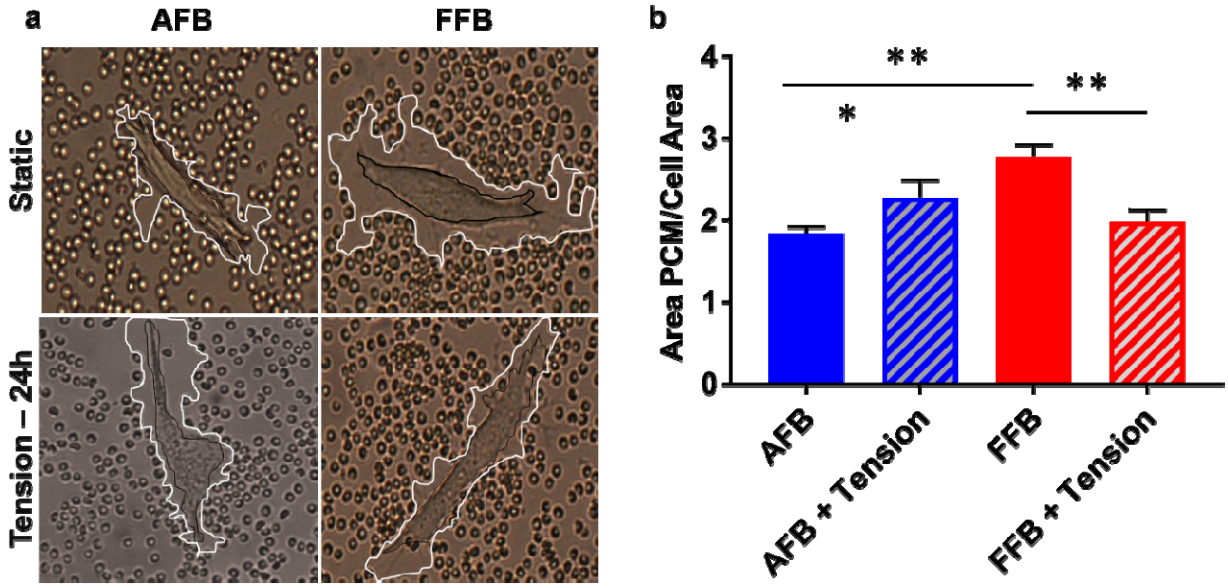
a
AFB
FFB
Static
Tension – 24h
b
Area PCM/Cell Area
0
1
2
3
4
*
**
**
AFB
AFB + Tension
FFB
FFB + Tension

Figure 2

Figure 3

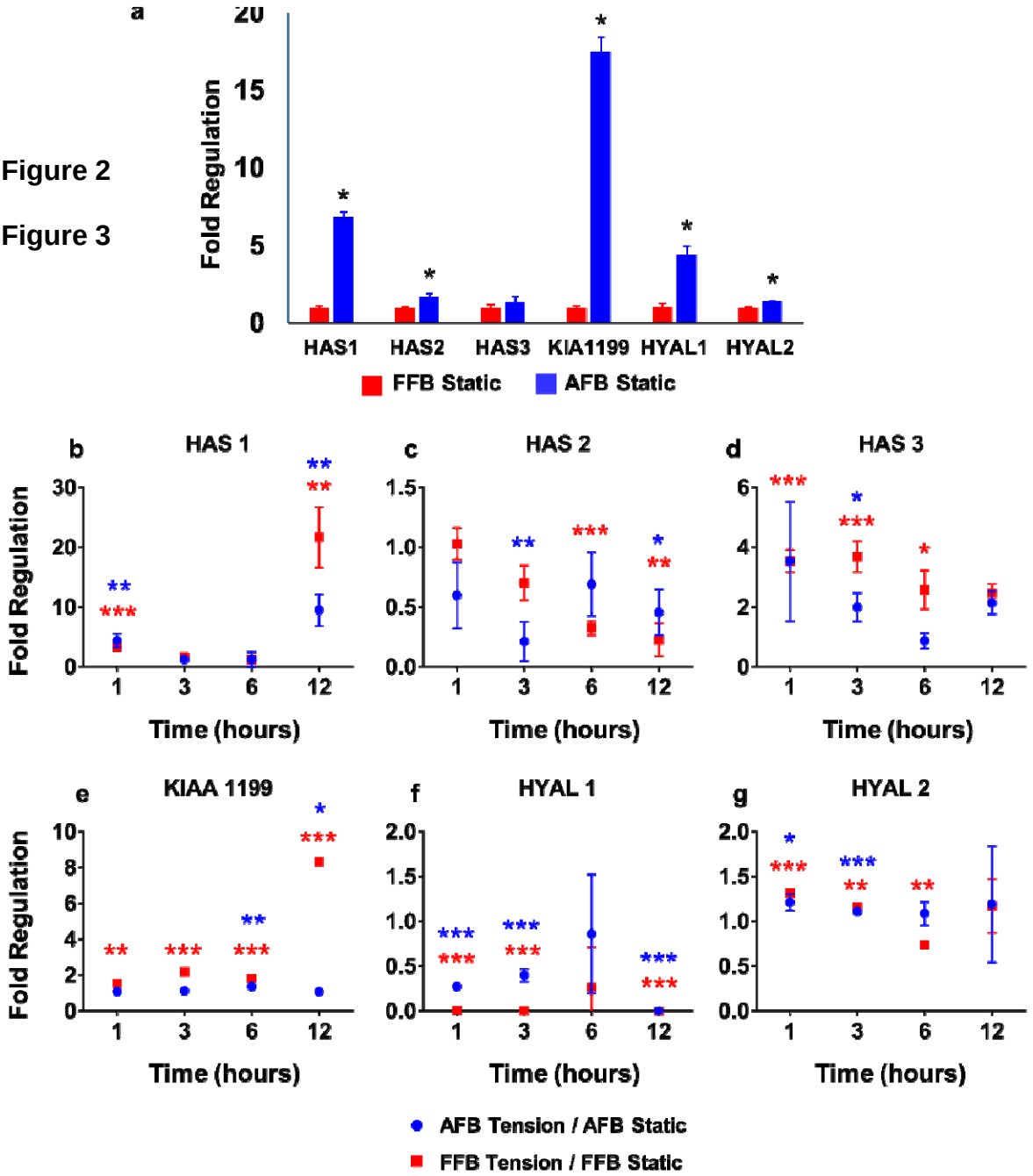

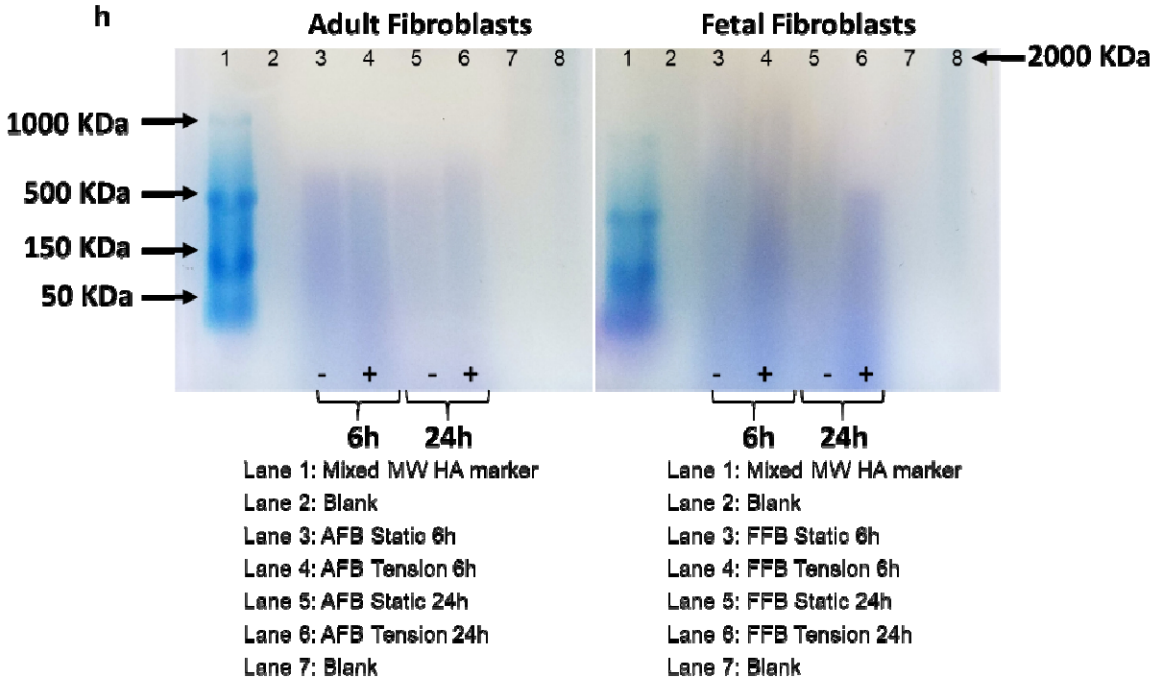

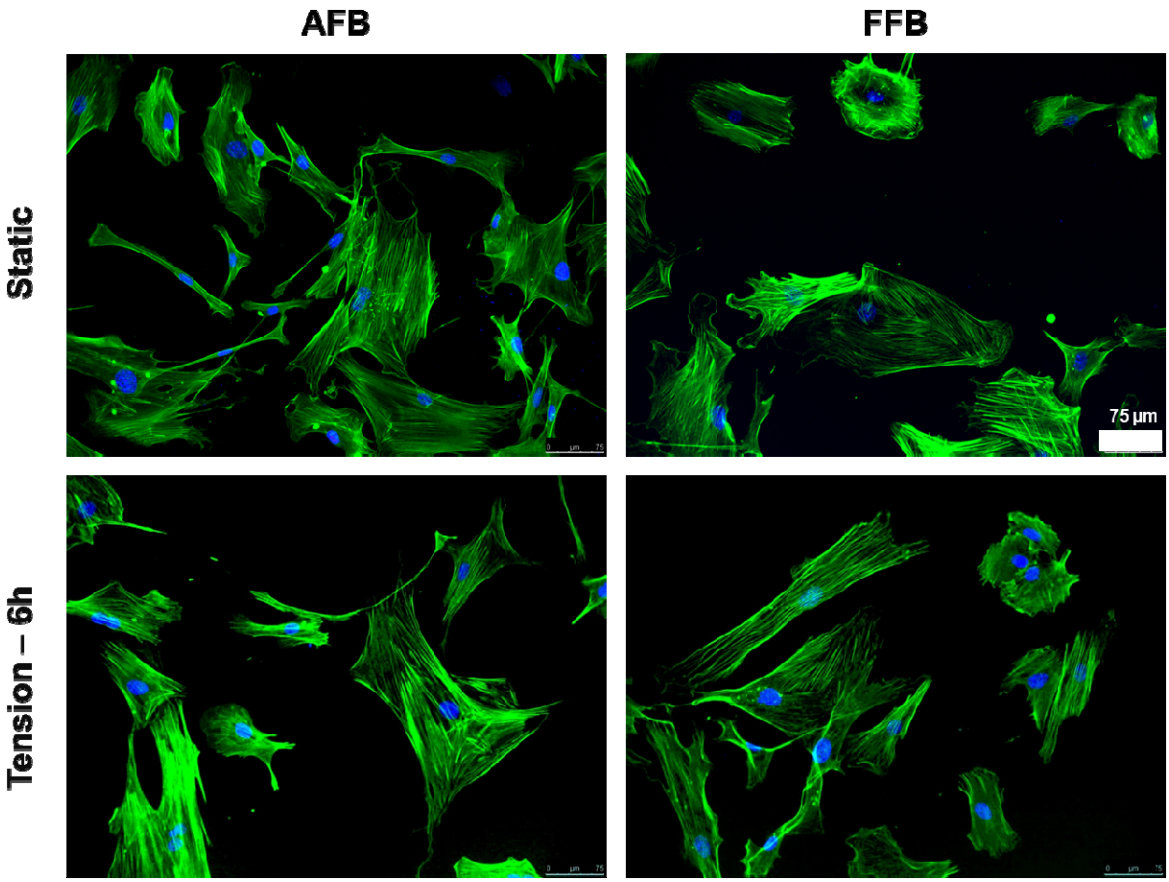
AFB
FFB
Static
Tension – 6h
75 µm

Figure 4

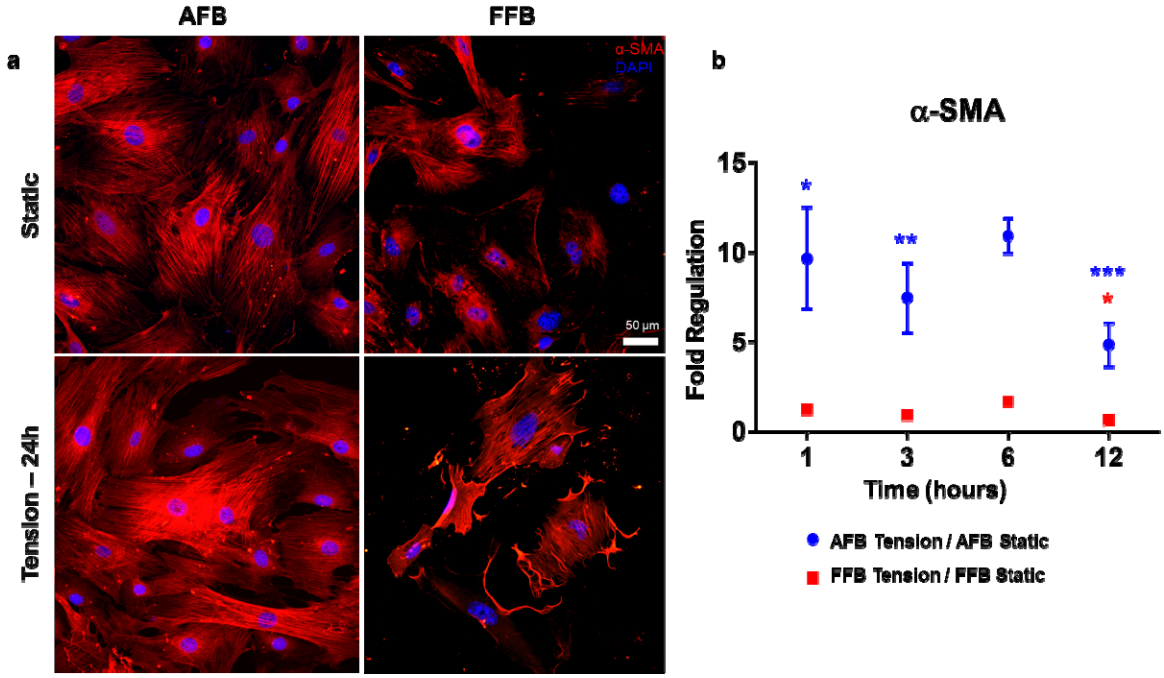
AFB
FFB
a
Static
Tension – 24h
α-SMA
DAPI
50 µm
b
α-SMA
Fold Regulation
15
10
5
0
1
3
6
12
Time (hours)
*
**
***
*
AFB Tension / AFB Static
FFB Tension / FFB Static

Figure 5

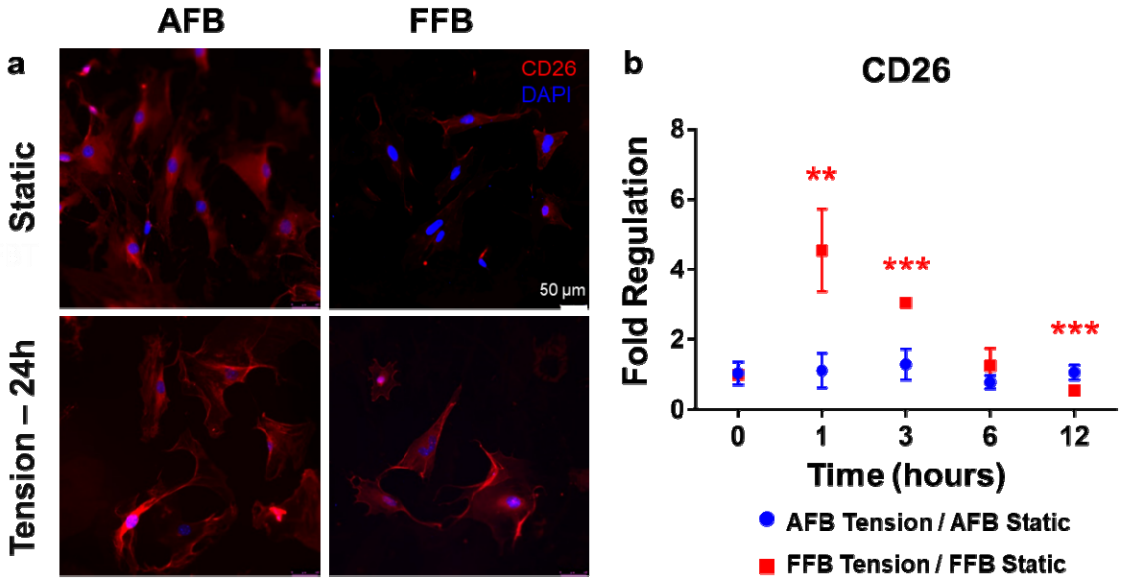
AFB
FFB
a
Static
Tension – 24h
CD26
DAPI
50 µm
b
CD26
Fold Regulation
8
6
4
2
0
**
***
***
0
1
3
6
12
Time (hours)
AFB Tension / AFB Static
FFB Tension / FFB Static

Figure 6

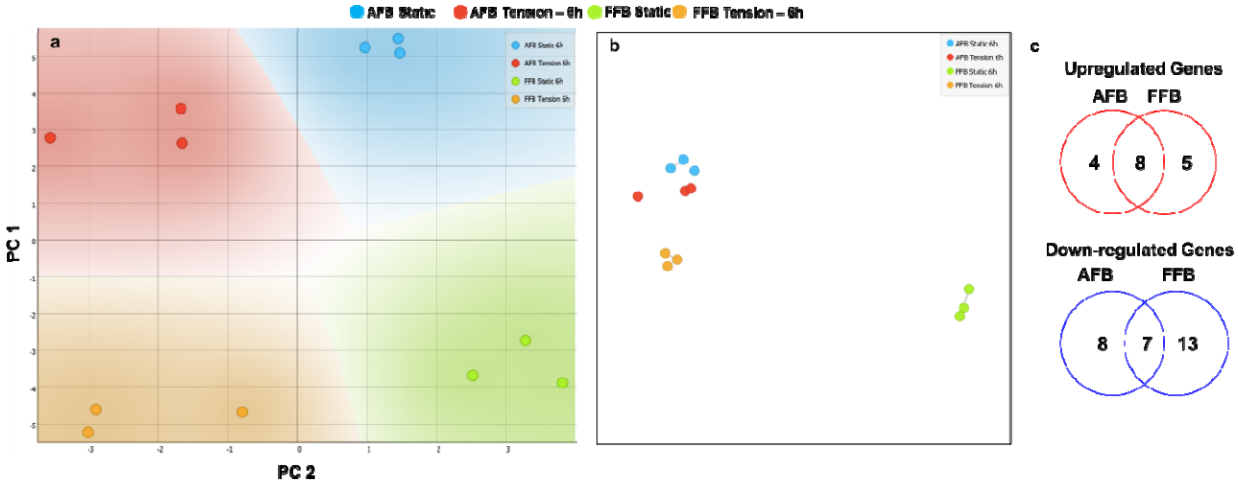
AFB Static
AFB Tension – 6h
FFB Static
FFB Tension – 6h
a
PC 1
PC 2
b
c
Upregulated Genes
AFB
FFB
4
8
5
Down-regulated Genes
AFB
FFB
8
7
13

Figure 7

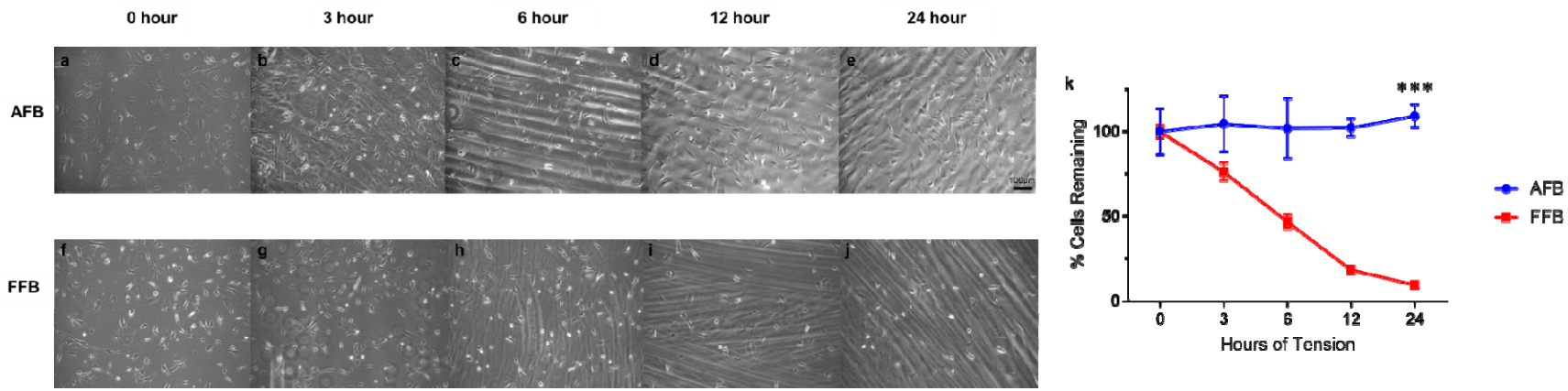
0 hour
3 hour
6 hour
12 hour
24 hour
AFB
FFB
a
b
c
d
e
f
g
h
i
j
k
***
% Cells Remaining
100
50
0
0
3
6
12
24
Hours of Tension
AFB
FFB

Figure 8

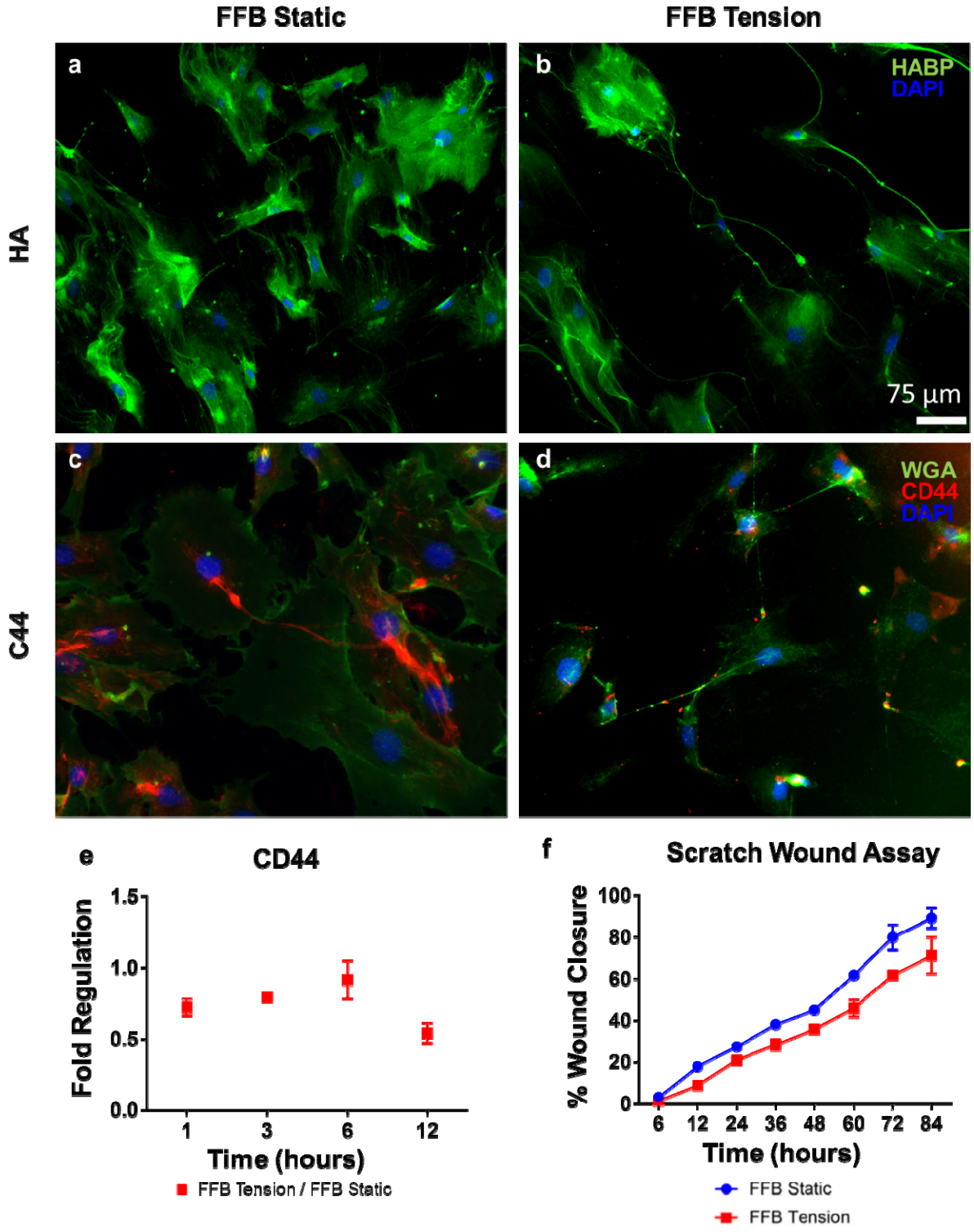
FFB Static
FFB Tension
HA
C44
a
b
HABP
DAPI
75 µm
c
d
WGA
CD44
DAPI
e
CD44
Fold Regulation
1.5
1.0
0.5
0.0
1
3
6
12
Time (hours)
FFB Tension / FFB Static
f
Scratch Wound Assay
% Wound Closure
100
80
60
40
20
0
6
12
24
36
48
60
72
84
Time (hours)
FFB Static
FFB Tension